Statistical Structure of Polarization-Inhomogeneous Images of Biotissues with Different Morphological Structures

Yu.A. Ushenko

Chernivtsi National University, 2 Kotsyubinsky St., 58012 Chernivtsi, Ukraine,
ushenko-bio@itf.cv.ukrtel.net

Received: 18.03.2005

Abstract

We investigate statistical polarization structure of the images of biological tissues with different morphological structures. The results for polarization coordinate mapping and the statistics of first-to-fourth orders performed for the polarization azimuth and ellipticity characterising biological tissues are outlined.

Keywords: polarization, statistical moments, biological tissue, optical birefringence

PACS: 42.62.-b, 42.62.Be, 42.25.Lc, 42.25.Ja, 81.70.Tx

1. Introduction

Optical methods for researching the structure of biological tissue (BT) may be historically divided into three main groups:

- spectrophotometric methods [1-3] based on the analysis of spatial (r) (or temporal (τ)) changes in the field intensity of the radiation scattered by BT;
- polarization methods that use a coherence matrix $\{\mathrm{K}(r,\tau)\}$ for the light oscillations [4-6],

$$\mathrm{K}(r,\tau)=\begin{Vmatrix}\langle E_x(r,\tau)E_x^*(r,\tau)\rangle & \langle E_x(r,\tau)E_y^*(r,\tau)\rangle\\ \langle E_x{}^*(r,\tau)E_y(r,\tau)\rangle & \langle E_y(r,\tau)E_y^*(r,\tau)\rangle\end{Vmatrix} \quad (1)$$

- and are based on the analysis of polarization degree $P(r)$ as a correlation function between the complex orthogonal components of electromagnetic oscillations E_x, E_y at the first point (r) of scattered radiation field [7],

$$P(r)=\sqrt{1-\frac{4\left\|\left[\left\langle E_x(r,\tau)E_x^*(r,\tau)E_y(r,\tau)E_y^*(r,\tau)\right\rangle-\left\langle E_x(r,\tau)E_y^*(r,\tau)E_y(r,\tau)E_x^*(r,\tau)\right\rangle\right]\right\|}{\left[\left\langle E_x(r,\tau)E_x^*(r,\tau)\right\rangle+\left\langle E_y(r,\tau)E_y^*(r,\tau)\right\rangle\right]^2}}; \quad (2)$$

correlation methods employing a correlation degree J for the parallel polarization components $E_x(r_1)$, $E_x(r_2)$ of the light oscillations at different points of the object field (r_1, r_2) [7-8],

$$J=\frac{\left\langle E_x(r_1,\tau)E_x{}^*(r_2,\tau)\right\rangle-\left\langle E_x{}^*(r_1,\tau)E_x(r_2,\tau)\right\rangle}{\left\langle E_x(r_1,\tau)E_x{}^*(r_2,\tau)\right\rangle+\left\langle E_x{}^*(r_1,\tau)E_x(r_2,\tau)\right\rangle}. \quad (3)$$

This paper deals with the methods of analysis for the measured 2D distributions of polarization azimuth and ellipticity (or the so-called polarization maps, PM) for the BT speckle-images, with the aim of searching for their interrelationships with the orientation morphological structure of birefringent architectonic nets. This represents a generalization of both the polarization and correlation methods mentioned above.

2. Theoretical Modelling

The analysis of PM of the BT images is based on the approach that allows morphological presentation of these bioobjects and uses the two-component ("amorphous" $\{A\}$ and "crystalline" $\{C\}$) matrix. The optical properties of the components can be described by the following Jones operators [9]:

$$\{A\}=\begin{Vmatrix}\exp(-\chi l) & 0\\ 0 & \exp(-\chi l)\end{Vmatrix}, \tag{4}$$

$$\{C\}=\begin{Vmatrix}\cos^2\rho+\sin^2\rho\exp(-i\delta); & \cos\rho\sin\rho[1-\exp(-i\delta)]\\ \cos\rho\sin\rho[1-\exp(-i\delta)]; & \sin^2\rho+\cos^2\rho\exp(-i\delta)\end{Vmatrix}, \tag{5}$$

where χ is the absorption coefficient of the amorphous BT layer with geometrical thickness l, ρ the package direction of the birefringent fibrils in the plane of BT sample, whose substance (i.e., fibrils) brings the phase shift δ for orthogonally polarised components E_{0x} and E_{0y} of the illuminating laser beam.

According to Eqs. (4) and (5), the amplitude-phase structure of the imaging amorphous and crystalline BT components can be described analytically with the following matrix equations:

$$\begin{pmatrix}E_x^A(r_A)\\ E_y^A(r_A)\end{pmatrix}=\{A\}\begin{pmatrix}E_{0x}\\ E_{0y}\end{pmatrix}, \tag{6}$$

$$\begin{pmatrix}E_x^C(r_C)\\ E_y^C(r_C)\end{pmatrix}=\{C\}\begin{pmatrix}E_{0x}\\ E_{0y}\end{pmatrix}, \tag{7}$$

where $\left[E_x^A(r_A),E_y^A(r_A)\right]$ and $\left[E_x^C(r_C),E_y^C(r_C)\right]$ are complex amplitudes of the electric field vectors of orthogonally polarised laser oscillations at the point r_A of "amorphous" and point r_C of "crystalline" (or architectonic [9]) constituent parts of the BT image.

Let us consider for simplicity polarization structure of the BT image, which is formed in case of probing the BT by linearly polarised laser beam with the azimuth $\alpha=0^0$ with respect to the inclination plane, when we have $\begin{pmatrix}E_{0x}\\ 0\end{pmatrix}$. Taking Eqs. (4) and (5) into account, one can rewrite the complex amplitudes of laser oscillations for the "amorphous" and "crystalline" components of the BT image as follows:

$$E_x^A(r)=E_{0x}\exp(-\chi l),\quad E_y^A(r)=0, \tag{8}$$

$$\begin{aligned}E_x^C(r)&=E_{0x}\left[\cos^2\rho(r)+\sin^2\rho(r)\exp(-i\delta(r))\right],\\ E_y^C(r)&=E_{0x}\left[\cos\rho(r)\sin\rho(r)(1-\exp(-i\delta(r)))\right].\end{aligned} \tag{9}$$

In order for determining local states of the light polarization at the points of BT image, let us write out the coherence matrices of the "amorphous" $\{\mathrm{K}^A(r)\}$ and "crystalline" $\{\mathrm{K}^C(r)\}$ constituent parts:

$$\{\mathrm{K}^A(r)\}=E_{0x}^2\begin{Vmatrix}\exp(-\chi l) & 0\\ 0 & 0\end{Vmatrix}, \tag{10}$$

$$\{\mathrm{K}^C(r)\}=\begin{Vmatrix}E_x^C(r)E^{*C}_x(r) & E_x^C(r)E_y^{*C}(r)\\ E_x^{*C}(r)E_y^C(r) & E_y^C(r)E_y^{*C}(r)\end{Vmatrix}. \tag{11}$$

According to Eqs. (10) and (11), the coordinate distribution of the polarization azimuth $\alpha(r_i)$ and the ellipticity $\beta(r_i)$ for the BT image is represented by the two PM types, (i) polarization-homogeneous PM

$$\begin{cases}\alpha^A(r_i)=0^0,\\ \beta^A(r_i)=0^0,\end{cases} \tag{12}$$

and (ii) polarization-inhomogeneous one

$$\begin{cases}\alpha^C(r_i)=\dfrac{1}{2}\arctan\dfrac{q_2}{q_1},\\ \beta^C(r_i)=\dfrac{1}{2}\arcsin\left[\dfrac{iq_2}{\sqrt{q_1+q_2+q_3}}\right],\end{cases} \tag{13}$$

where

$$q_1 = \left[E_x^C(r_i) E^{*C}_x(r_i) - E_y^C(r_i) E_y^{*C}(r_i) \right]^2,$$
$$q_2 = \left[E_x^C(r_i) E^{*C}_y(r_i) - E_x^{*C}(r_i) E_y^C(r_i) \right]^2, \quad (14)$$
$$q_3 = i\left[E_x^C(r_i) E^{*C}_y(r_i) - E_x^{*C}(r_i) E_y^C(r_i) \right]^2$$

Here $r_i \equiv \begin{pmatrix} r_1,...r_m \\ ..... \\ r_n,...r_m \end{pmatrix}$ is a set of BT image coordinates defined by the pixel amount of recording area of CCD camera.

3. Analysis and Discussion of Experimental Data

The optical scheme for measuring the PM is presented in Fig. 1. The BT was illuminated with the collimated (∅ = 10^4μm) He-Ne laser beam (λ=0.6328μm, W=5.0mW). Polarization illuminator consisted of quarter-wave plates 3 and 5 and polarizer 4, which formed the illuminating beam with random polarization azimuths ($0^0 \le \alpha_0 \le 180^0$) or ellipticities ($0^0 \le \beta_0 \le 90^0$). Polarised BT images were projected with microscope objective 7 onto the plane of light-sensitive platform (800×600 pixels) of CCD camera 9. This provided measuring range 2–2000 μm for the structural BT elements.

Experimental conditions were selected so as to eliminate spatial and angular aperture filtrations, while forming the BT image. This was ensured by matching the angular indicatrix characteristics of light scattering from the BT samples ($\Omega_{DS} \approx 16^0, \Omega_{MT} \approx 13^0$, where Ω_{DS} and Ω_{MT} are the plane angles of cones where 98% of the total energy of scattered radiation is concentrated) and the angular aperture of the microscope objective ($\Delta\omega = 20^0$). Finally, the BT images were analysed using analyser 8.

The methodology for determining the BT's PM consisted in the following sequence of actions:

1. While using CCD 9, without the analyser 8, one can measure an array of intensities of the BT image $I\begin{pmatrix} r_1,...r_m \\ ..... \\ r_n,...r_m \end{pmatrix}$.
2. Then one inserts the analyser 9, whose transmission axis is in series oriented at angles $\Theta = 0^0$ and $\Theta = 90^0$, and measures the arrays of intensities $I^{(0)}\begin{pmatrix} r_1,...r_m \\ ..... \\ r_n,...r_m \end{pmatrix}$ and $I^{(90)}\begin{pmatrix} r_1,...r_m \\ ..... \\ r_n,...r_m \end{pmatrix}$.
3. By rotating analyser axis Θ within the range $\Theta = 0 \div 180^0$, one can find the arrays of minimum and maximum intensity levels $I_{\min}\begin{pmatrix} r_1,...r_m \\ ..... \\ r_n,...r_m \end{pmatrix}$ and $I_{\max}\begin{pmatrix} r_1,...r_m \\ ..... \\ r_n,...r_m \end{pmatrix}$ for each individual pixel (*mn*) of the CCD camera and the corresponding rotation angles $\Theta\begin{pmatrix} r_1,...r_m \\ ..... \\ r_n,...r_m \end{pmatrix}$ (where $I\begin{pmatrix} r_1,...r_m \\ ..... \\ r_n,...r_m \end{pmatrix} \equiv I_{\min}$).
4. Finally, one could calculate the PM of the BT image by using the relationships

$$\alpha\begin{pmatrix} r_1,...r_m \\ ..... \\ r_n,...r_m \end{pmatrix} = \Theta\left(I(r_i) \equiv I_{\min}\right) - \frac{\pi}{2},$$
$$\beta\begin{pmatrix} r_1,...r_m \\ ..... \\ r_n,...r_m \end{pmatrix} = \arctan\frac{I(r_i)_{\min}}{I(r_i)_{\max}}. \quad (15)$$

"Optically thin" ($\tau \le 0.1$) histological BT cuts with different morphological structures were used as research objects, in particular, a muscular tissue (myocardium) or MT (see Fig. 2a and 2b), a kidney tissue or KT (see Fig. 2c and 2d) and a spleen tissue or ST (see Fig. 2e and 2f). The objects under test had similar optically anisotropic component, with the birefringence $\Delta n \approx 1.5 \times 10^{-3}$ visualised in crossed polarizers (Fig. 2b, 2d and 2f). The

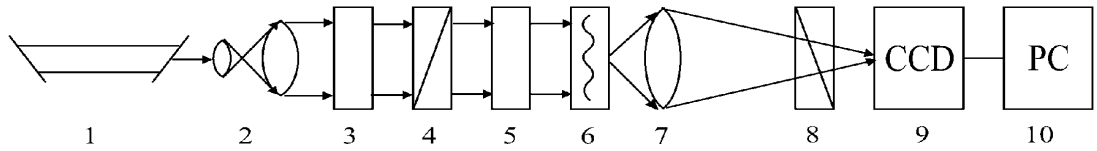

Fig. 1. Optical scheme for measuring PM of speckle-images for BT: 1, He-Ne laser; 2, collimator; 3 and 5, quarter-wave plates; 4, polarizer; 8, analyser; 6, object under test; 7, microobjective; 9, CCD camera; 10, personal computer.

morphological architectonic structures of such the BT are different. The MT is formed by "quasi-ordered" bundles of birefringent myosin bundles (Fig. 2b). The KT architectonics is linked to collagen fibres oriented chaotically (Fig. 2d). Finally, the ST includes "island" inclusions of anisotropic collagen (Fig. 2f). The sample selection described above made it possible to analyse the influence of orientation architectonics of physiologically different BT upon the PM speckle-image structures.

The experimental part contains collecting the PM $\alpha\begin{pmatrix} r_1,...r_m \\ ..... \\ r_{n;},...r_m \end{pmatrix}$ and $\beta\begin{pmatrix} r_1,...r_m \\ ..... \\ r_n,...r_m \end{pmatrix}$ of speckle-images for all the types of BT (see Fig.3a, 3b to Fig. 5a, 5b), the probability distributions W of polarization azimuth $\alpha(r_i)$ and ellipticity $\beta(r_i)$, as well as their statistical moments of first to fourth orders (see Fig. 3c, 3d to Fig. 5c, 5d and Table 1).

Table 1. Statistics of polarization states of the BT images.

MT (37 samples)				KT (34 samples)				ST (35 samples)			
$\alpha(r_i)$		$\beta(r_i)$		$\alpha(r_i)$		$\beta(r_i)$		$\alpha(r_i)$		$\beta(r_i)$	
M_α	0.38	M_β	0.24	M_α	0.29	M_β	0.18	M_α	0.11	M_β	0.08
σ_α	0.25	σ_β	0.21	σ_α	0.18	σ_β	0.16	σ_α	0.06	σ_β	0.05
A_α	93.8	A_β	89.7	A_α	79.4	A_β	68.3	A_α	20.4	A_β	16.1
E_α	981.6	E_β	832.0	E_α	682.7	E_β	574.2	r_C	11.4	E_β	8.25

The comparative analysis of the data obtained yields in the next conclusions:

(i) The coordinate PM structure of the MT speckle-images (see Fig. 3a and 3b) might be considered as representing ensembles of large-scale (100–200 μm) mono-polarised ($\{\alpha(r_i),\beta(r_i)\}\approx const$) regions (or polarization domains). The areas of similar polarization for the KT images (Fig. 4a and 4b) are smaller-scale (25–100 μm) and have rather chaotic form. The PM of ST (Fig. 5a and 5b) are formed by polarised parts of small sizes (5–20 μm) and are located in equi-probable enough manner in the plane of image.

(ii) Histograms $W(\alpha)$ and $W(\beta)$ (see Fig. 3c, 3d to Fig. 5c, 5d) characterise the probability distributions for the polarization parameters $\{\alpha(r_i),\beta(r_i)\}$ of the BT images. A peculiar feature of the MT is neatly pronounced $W(\alpha)$ and $W(\beta)$ extremes (Fig. 3c and 3d). They point to statistical prevalence of certain polarization states in the laser image. The PM histograms of the KT images (see Fig. 4c and 4d) are formed by a series of local extremes situated in a wider range of polarization parameters $\{\alpha(r_i),\beta(r_i)\}$. The probability polarization structure of the ST image (Fig. 5c and 5d) is determined by superposition of two components: a polarization-homogeneous one, coinciding with the polarization state of illuminating beam

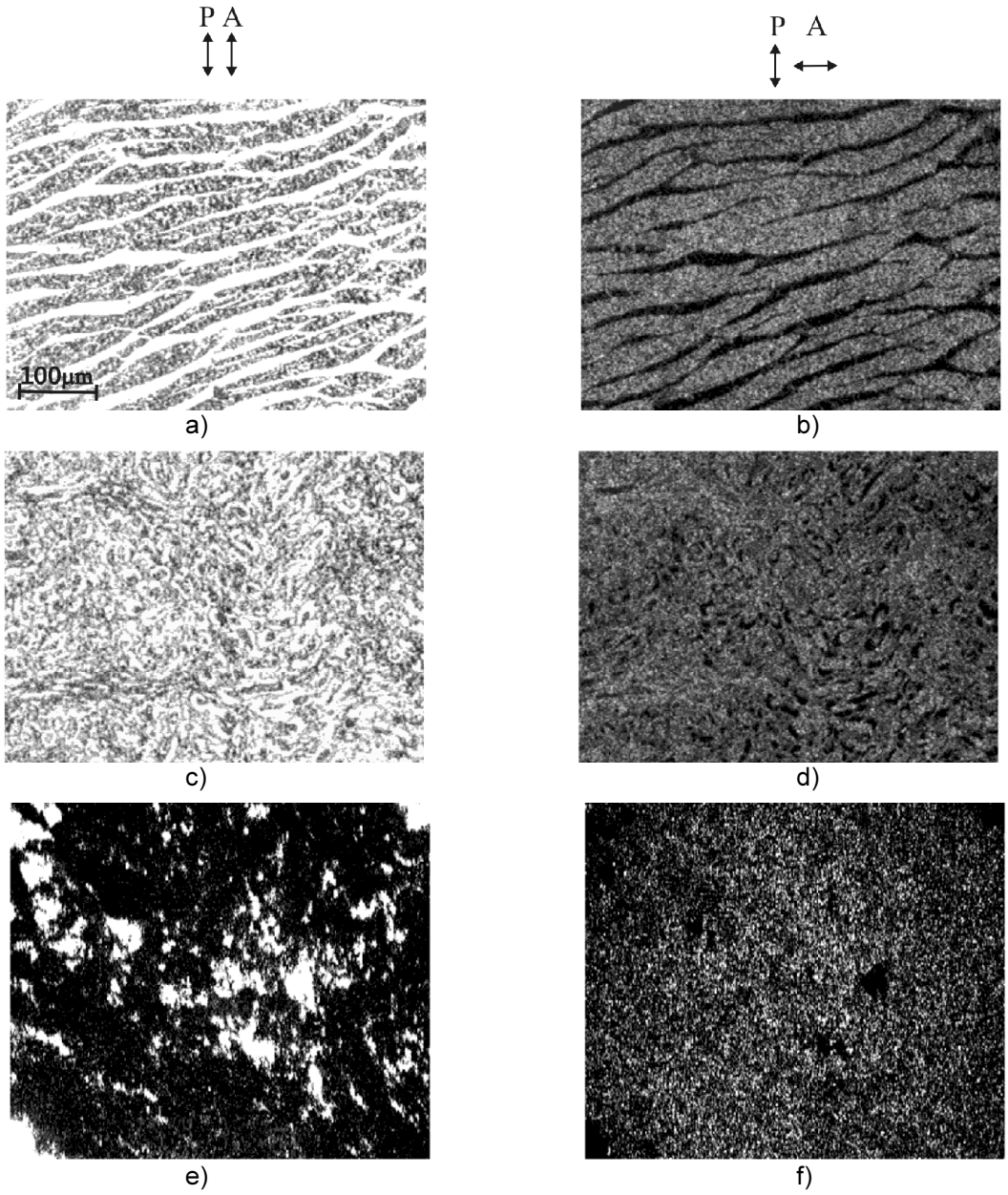

Fig. 2. Coherent images for different types of BT obtained in parallel (left-side images) and crossed (right-side images) polarizers: MT (a, b), KT (c, d) and ST (e, f)). The arrows show orientations of the transmission axes of polarizer (A) and analyser (B).

($\alpha_0 = 0^0$, $\beta_0 = 0^0$), and a polarization-inhomogeneous one. The first PM component is characterised by clearly expressed histogram extremes $W(\alpha)$ and $W(\beta)$, and the second one by a set of local small-value extremes.

(iii) The dependences $W(\alpha)$ and $W(\beta)$ are well characterised by a set of statistical moments of first-to-fourth orders associated with the azimuths and ellipticities. They are calculated using the relations

$$M_{\alpha,\beta} = \frac{1}{N}\sum_{i=1}^{N}|z_i|,\ \sigma_{\alpha,\beta} = \sqrt{\frac{1}{N}\sum_{i=1}^{N}z_i^2},$$
$$A_{\alpha,\beta} = \frac{1}{\sigma_S^3}\frac{1}{N}\sum_{i=1}^{N}z_i^3,\ E_{\alpha,\beta} = \frac{1}{\sigma_S^2}\frac{1}{N}\sum_{i=1}^{N}z_i^4, \quad (16)$$

where $N = m \times n$ is the overall amount of CCD camera pixels, and z_i corresponds to α_i or β_i parameters.

The values of parameters figuring in Eq. (17), averaged over statistically reliable amount of the BT samples of all types, are gathered in Table 1.

The PM structure of the BT of different types may be concerned with the following peculiarities of morphological structure of their architectonics. The MT structures transforming

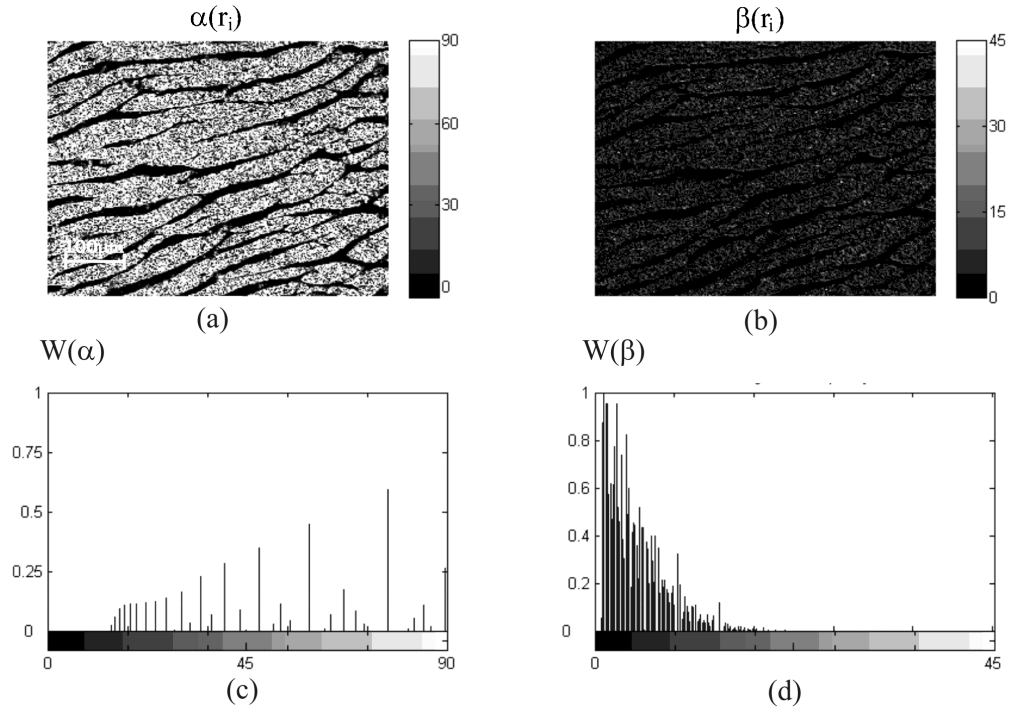

Fig. 3. PM of azimuth (a) and ellipticity (b) of the MT speckle-images and their probability structures (c, d).

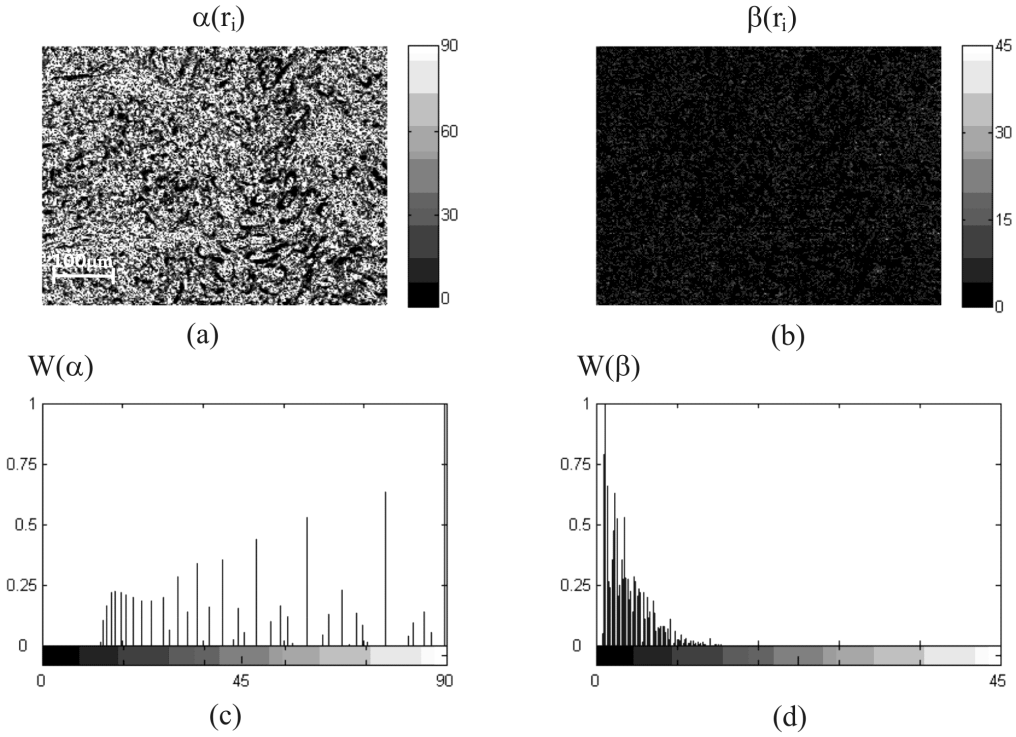

Fig. 4. PM of azimuth (a) and ellipticity (b) of the KT speckle-images and their probability structures (c, d).

laser polarization are large-scale domains of "mono-oriented" myosin fibres. According to Eqs. (14) and (15), the coordinate distributions of the polarization azimuth $\alpha\begin{pmatrix} r_1,...r_m \\ ..... \\ r_n,...r_m \end{pmatrix}$ and ellipticity $\beta\begin{pmatrix} r_1,...r_m \\ ..... \\ r_n,...r_m \end{pmatrix}$ turn out to be homogeneous within the domains, where $\rho,\delta\begin{pmatrix} r_l,...r_k \\ ..... \\ r_g,...r_q \end{pmatrix}_{1\le l,k,g,q\le m,n} \approx const$ (Fig. 3a and 3b), and the corresponding histograms $W(\alpha)$ and $W(\beta)$ have marked extremes (see Fig. 3c and 3d).

A wide spectrum of angles between the polarization azimuth of illuminating beam α_0 and local directions ρ is inherent for the case of the KT architectonic net, which is formed by chaotically oriented collagen fibres. Hence, the areas of identical polarization decrease (Fig. 4a and 4b) and their corresponding histograms may be represented as sets of a great number of local extremes (Fig. 4c and 4d).

The anisotropic component in case of the ST does not have a definite fibrous or fibrillar structure. Therefore, polarization-inhomogeneous component of its speckle-images is characterised by polarization azimuths and ellipticities distributed equi-probably enough (see Fig. 5a and 5b). The corresponding probabilities are order of magnitude less than those of the polarization parameters for illuminating laser beam (Fig. 5c and 5d).

The information on the statistical moments of first-to-fourth orders characterising the distributions $W(\alpha)$ and $W(\beta)$ for speckle-images of different BT enables one to reach the conclusions expressed in terms of the following relations:

$$\begin{aligned} &M_{\alpha,\beta}(MT)\ge M_{\alpha,\beta}(KT)\ge M_{\alpha,\beta}(ST),\\ &\sigma_{\alpha,\beta}(MT)\ge \sigma_{\alpha,\beta}(KT)\ge \sigma_{\alpha,\beta}(ST),\\ &A_{\alpha,\beta}(MT)\ge A_{\alpha,\beta}(KT)\ge A_{\alpha,\beta}(ST),\\ &E_{\alpha,\beta}(MT)\ge E_{\alpha,\beta}(KT)\ge E_{\alpha,\beta}(ST). \end{aligned} \qquad (17)$$

It is clear that the character of the probability distributions peculiar for optical-

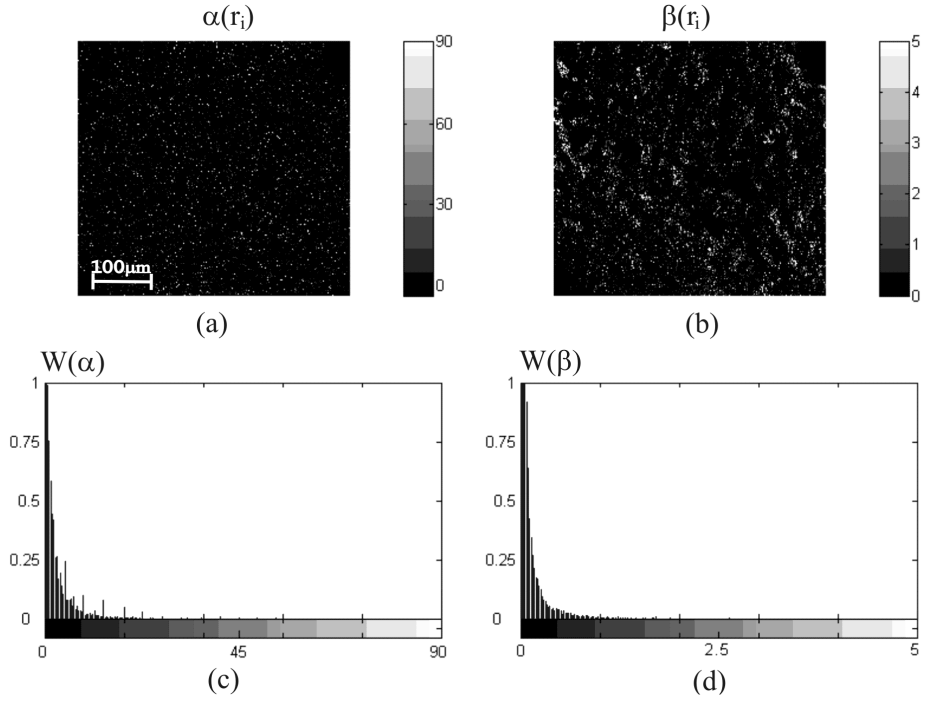

Fig. 5. PM of azimuth (a) and ellipticity (b) of the ST speckle-images and their probability structures (c, d).

geometrical parameters of the architectonic nets deviates from purely statistical (equi-probable or normal-law) towards a stochastic and self-similar one, with larger statistical moments for the polarization parameters.

Summing up, our main results lie in follows:

- the technique of polarization mapping of the images of BT with different morphological structures is experimentally approved;
- the coordinate and statistical structures (in particular, the average, dispersion, the skewness and the kurtosis) of 2D distributions of light polarization azimuths and ellipticities at different points of the BT images are analysed on the basis of two-component optically anisotropic model of BT architectonics;
- it is revealed that the statistical moments of the azimuths and ellipticities of third and fourth orders are the most sensitive to the orientation structure of BT architectonics and so diagnostically important.

References

1. Patterson M. S., Andersson-Engels S., Wilson Brian C., and Osei E.K., Appl. Opt. **34**, 22 (1995).
2. Alfano R.R. and FujimotoJ.G., Eds., Advances in Optical Imaging and Photon Migration, Vol. 2 of Topics in Optics and Photonics Series (Optical Society of America, Washington, D. C., 1996).
3. Bartel S. and Hielscher A.H., Appl. Opt. **39**, 1580 (2000).
4. Morgan S.P., Khong M.P., and Somekh M.G., Appl. Opt. **36**, 1560 (1997).
5. Demos S.G. and Alfano R.R., Appl. Opt. **36**, 150 (1997)
6. Jacques S.L., Roman J.R., and Lee K., Lasers in Surg. & Med. **26**, 119 (2000).
7. Huang D., Swanson E.A., Lin C.P., Schuman J.S., Stinson W.G., Chang W., Hee M.R., Flotte T., Gregory K., Puliafito C.A., and Fujimoto J., Science **254**, 1178 (1991).
8. Ushenko A.G., and Pishak V.P., “Laser Polarimetry of Biological Tissue. Principles and Applications” in Coherent-Domain Optical Methods. Biomedical Diagnostics, Environmental and Material Science (V.Tuchin, Ed.), Kluwer Academic Publishers, 2004. – P.67 – 93.
9. Angelsky O.V., Demyanovsky G.V., Ushenko A.G., Burcovets D.N., and Ushenko Yu.A., Wavelet analysis of two-dimensional birefringence images of architectonics in biotissues for diagnosing pathological changes, J. Biomed. Opt., **9**, 679 (2004).